An algebraic model for the kinetics of covalent enzyme inhibition at low substrate concentrations

ACCEPTED FOR PUBLICATION Nov 17, 2014

Petr Kuzmič*[,a], James Solowiej[b], Brion W. Murray[b]

[a] *BioKin Ltd., Watertown, Massachusetts*
[b] *Oncology Research Unit, Pfizer Worldwide Research and Development, La Jolla, California*

Abstract

This report describes an integrated rate equation for the time-course of covalent enzyme inhibition under the conditions where the substrate concentration is significantly lower than the corresponding Michaelis constant, such as for example in the Omnia® assays of EGFR kinase. The newly described method is applicable to experimental conditions where the enzyme concentration is significantly lower than the dissociation constant of the initially formed reversible enzyme-inhibitor complex (no "tight binding"). A detailed comparison with the traditionally used rate equation for covalent inhibition is presented. The two methods produce approximately identical values of the first-order inactivation rate constant (k_{inact}). However, the inhibition constant (K_{i}) and therefore also the second-order inactivation rate constant $k_{\mathrm{inact}}/K_{\mathrm{i}}$, is underestimated by the traditional method by up to an order of magnitude.

Key words: enzyme kinetics; theory; mathematics; covalent inhibition; irreversible inhibition; EGFR kinase

Contents

*Corresponding author contact: `http://www.biokin.com`

1. INTRODUCTION

Covalent enzyme inhibition has both reversible and irreversible components. The reversible component is analogous to the equilibrium constant for simple reversible inhibitors (K_i). In a subsequent step, characterized by the rate constant k_inact, a covalent bond is formed irreversibly. Characterizing these two contributions to covalent inhibitor potency is essential to understand their biological impact as well as in the design of more effective drugs.

In a recent report [1] we described a detailed kinetic analysis of covalent (irreversible) inhibition of the EGFR kinase under the special experimental conditions where the peptide substrate concentration, $[S]_0$, is very much lower than the corresponding Michaelis constant, $K_\mathrm{M,Pep}$. The mathematical model consisted of a system of simultaneous first-order ordinary differential equations (ODE), which must be integrated numerically in order to compute the reaction time course. Two important advantages of ODE models in enzyme kinetics are that all conceivable molecular mechanisms can be treated and that no simplifying assumptions are made regarding the experimental conditions. One important disadvantage is that the iterative numerical integration of ODE systems is a relatively tedious and time consuming task, which can only be accomplished by utilizing highly specialized software packages such as DynaFit [2, 3].

Here we describe a simple algebraic equation that can be used, instead of a full ODE system, to analyze covalent inhibition kinetics. This integrated rate equation is applicable under two simultaneously satisfied simplifying assumptions. First, as was the case in the previous report [1], we require that the substrate concentration must be very much lower than the corresponding Michaelis constant. Second, the enzyme concentration must be very much lower than the inhibition constant that characterizes the initially formed noncovalent enzyme-inhibitor complex. The second requirement is equivalent to saying that there is no "tight binding" [4, 5, 6, 7, 8, 9, 10].

Results obtained by using the newly presented method were compared with those obtained by using the conventionally applied kinetic model of covalent enzyme inhibition (see for example ref. [11, Chap. 9]). We show that ignoring what many casual observers would consider a "minor" nonlinearity in the no-inhibitor control can cause up to almost one order of magnitude distortion in the best-fit values of K_i and $k_\mathrm{inact}/K_\mathrm{i}$. Interestingly, the best-fit value of k_inact obtained by the conventional mathematical model under low substrate concentrations (relative to the K_M) shows only a minor distortion.

2. MATERIAL AND METHODS

2.1. Experimental

The expression and purification of EGFR L858R/T790M double mutant, as well as the determination of active enzyme concentration, is described elsewhere [1]. Fluorometric assays were performed by using the Omnia® continuous fluorometric kinase assay system (Invitrogen, Carlsbad, California) using peptide Y-12, a fluorogenic tyrosine phosphoacceptor peptide modified with a chelation-enhanced fluorophore (cSx) coupled to a cysteine residue, Ac-EEEEYI(cSx)IV-NH_2. Phosphopeptide formation was monitored in 50 μL reactions in 96-well plates with a Tecan Safire II microplate reader in fluorescence mode using 360 nm excitation and 485 nm emission wavelengths. Reactions were comprised of 12 mM free $MgCl_2$, 1 mM DTT, 13 μM peptide-cSx, 800 μM ATP, 150 mM NaCl, and 0.01% Tween-20 in 50 mM HEPES pH 7.5. The reaction mixture contained various concentrations of the inhibitor identified as Compound 5 in ref. [1]. Reactions were initiated by the addition of 20 nM EGFR L858R/T790M (final concentration).

2.2. Mathematical

Covalent inhibition under first-order substrate conditions in the absence of "tight binding". Let us assume that (a) the substrate concentration, $[S]_0$, is very much lower than the corresponding Michaelis constant, K_M, and (b) the enzyme concentration, $[E]_0$, is very much lower than the inhibition constant, K_i, which characterizes the initially formed enzyme-inhibitor complex. It could be shown (see Appendix C) that under those particular limiting conditions the experimental signal such as fluorescence, F, changes over time, t, according to Eqn (1). In Eqn (1), F_0 is the baseline offset of the experimental signal, i.e., a property of the instrument; r_P is the molar response coefficient of the reaction product, i.e., the number of instrument units generated by one concentration unit of the reaction product being produced in the enzyme reaction. The symbols α, β represent auxiliary variables defined in Eqns (2), (3), respectively, where K_i is the apparent [4] inhibition constant depending on the presumed inhibition mechanism (e.g. competitive); k_inact is the first-order inactivation rate constant for the irreversible conversion of the initially formed noncovalent complex to the final covalent conjugate.

$$F = F_0 + r_\mathrm{P}\,[S]_0\,\{1 - \exp\left[-\beta\,(1 - \exp\left(-\alpha\,t\right))\right]\} \tag{1}$$

$$\alpha = k_\mathrm{inact}\,\frac{[I]_0}{[I]_0 + K_\mathrm{i}} \tag{2}$$

$$\beta = \frac{[E]_0\,k_\mathrm{sub}}{[I]_0}\,\frac{K_\mathrm{i}}{k_\mathrm{inact}} \tag{3}$$

Equation (1) was utilized either in the local fit mode, where each individual kinetic trace was analyzed separately, or in the global fit mode [12], where all kinetic traces obtained at different concentration of the inhibitor were combined and analyzed a single super-set of experimental data. In the local mode scenario, the optimized model parameters were α, β, and F_0, while the molar response factor r_P (determined independently) was held fixed at 5010 RFU/μM of phosphorylated product. In the global fit mode, the

globally optimized parameters were k_{inact}, K_{i}, k_{sub}, while the locally optimized parameters (specific for each individual data set) were the baseline offset F_0, and the six highest inhibitor concentrations, $[I]_0$.

Covalent inhibition under first-order substrate conditions in the presence or absence of "tight binding". To validate the performance of the newly derived integrated rate Eqn (1), we also performed a global fit of all combined kinetic traces at $[I]_0 > 0$ to the differential-equation model described elsewhere [1]. Briefly, the observed fluorescence F at reaction time t was modeled by using Eqn (4), where F_0 is the baseline offset; r_{P} is the molar response factor of the phosphorylated reaction product (5010 RFU/μM); and $[P]$ is the product concentration at time t.

$$
\begin{aligned}
F &= F_0 + r_{\mathrm{P}}\,[P] && (4)\\
\mathrm{d}[E]/\mathrm{d}t &= -k_{\mathrm{aI}}[E][I] + k_{\mathrm{dI}}[E.I] && (5)\\
\mathrm{d}[S]/\mathrm{d}t &= -k_{\mathrm{sub}}[E][S] && (6)\\
\mathrm{d}[P]/\mathrm{d}t &= +k_{\mathrm{sub}}[E][S] && (7)\\
\mathrm{d}[I]/\mathrm{d}t &= -k_{\mathrm{aI}}[E][I] + k_{\mathrm{dI}}[E.I] && (8)\\
\mathrm{d}[E.I]/\mathrm{d}t &= +k_{\mathrm{aI}}[E][I] - k_{\mathrm{dI}}[E.I] - k_{\mathrm{inact}}[E.I] && (9)\\
\mathrm{d}[E{\sim}I]/\mathrm{d}t &= +k_{\mathrm{inact}}[E.I] && (10)
\end{aligned}
$$

The product concentration $[P]$ was computed by numerical integration of the ODE system (5)-(10) using the LSODE integration algorithm [13]. All concentrations were scaled to micromolar units. The absolute local truncation error was kept below 10^{-14} μM; the relative local truncation error was kept below 10^{-8} (eight significant digits).

Conventional integrated rate equation for covalent inhibition. For comparison with the newly proposed method, individual kinetic traces were fit to Eqn (11), see ref. [11, Chapter 9].

$$
\begin{aligned}
F &= F_0 + r_{\mathrm{P}}\frac{v_i}{k_{\mathrm{obs}}}\left[1 - \exp\left(-k_{\mathrm{obs}}\,t\right)\right] && (11)\\
k_{\mathrm{obs}} &= k_{\mathrm{inact}}\frac{[I]_0}{[I]_0 + K_{\mathrm{i}}} && (12)
\end{aligned}
$$

Eqn (11) was utilized only in local fit mode. The optimized parameters were F_0, v_{i} and k_{obs}. As before, the molar response of phosphorylated product, r_{P}, was kept constant at 5010 RFU/μM.

First-order substrate kinetics. Reaction progress curves in the absence of inhibitor were fit to Eqn (13), where F is the observed fluorescence intensity and t is reaction time. The adjustable model parameters were the baseline offset, F_0, the maximum amplitude F_{max}, and the first-order rate constant k. The corresponding instantaneous rate curves were computed by using Eqn (14), which is obtained by differentiating Eqn (13) with respect to time.

$$F = F_0 + F_{\max}\left[1 - \exp\left(-k\,t\right)\right] \quad (13)$$

$$v \equiv \mathrm{d}F/\mathrm{d}t = F_{\max}\,k\,\exp\left(-k\,t\right) \quad (14)$$

2.3. Computational

All computations, using either algebraic or differential-equation models, were performed by using the software package DynaFit [2, 3]. Representative input code is listed in the Appendix. The raw experimental data utilized in this report are available for download from http://www.biokin.com.

3. RESULTS

Nonlinearity of the no-inhibitor control curve. A typical time course of an EGFR L858R/T790M assay in the absence of inhibitors is shown in *Fig* 1. The first ten minutes of the assay (*Fig* 1, Inset) appear distinctly linear upon visual inspection.

The solid curve in the upper panel of *Fig* 1 represents the least-squares fit of the experimental data to the exponential model defined by Eqn (13). The best-fit nonlinear model parameters were $F_0 = (26112 \pm 48)$ RFU, $F_{\max} = (45970 \pm 640)$ RFU, and $k = (0.000557 \pm 0.000011)$ s^{-1}. The corresponding residual plot, represented as grayed squares in the bottom panel of *Fig* 1. A runs-of-signs residual analysis was performed according to established methods [14, 15]. With 100 data points and 52 positive residuals, the predicted number of entirely random sign changes is 50 ± 5. The observed number of sign changes was 38, which corresponds to the p value of 0.004. Thus there is a certain degree of non-randomness exhibited graphically as an "inverted rainbow" pattern spanning the first approximately 500 seconds. This corresponds to a moderate lag phase seen in many Omnia® kinase assays.

The dashed straight line in the upper panel of *Fig* 1 represents the results linear least-squares fit. The best-fit model parameters were slope (reaction rate) 17.67 RFU/sec and intercept 27790 RFU. The coefficient of determination ("R-squared") was $R^2 = 0.989$. The corresponding residual plot is shown as filled circles in the lower panel of *Fig* 1. The residuals changed sign only 7 times, as opposed to 38 times in the exponential fit. With 100 data points and 52 positive residuals, merely 7 runs of signs correspond to a p value indistinguishable from zero (there is essentially zero likelihood that 100 coin tosses would produce only 7 runs of heads or tails). The residual plot has a distinctly rainbow or horseshoe shape characteristic of a significant lack of fit.

The smooth curve in *Fig* 2 shows the instantaneous exponential rate curve, i.e., the first-derivative of the exponential best-fit model in *Fig* 1 with respect to time. The instantaneous reaction rate decreases over the course of the 24-minute assay by more than 50%, from approximately 26 RFU/sec to approximately 11 RFU/sec. This level of decrease in the instantaneous rate indicates significant nonlinearity.

The linearity vs. nonlinearity of the control progress curve was also examined by the cross-validation method [16]. Accordingly, the control progress curve, comprised of 100 data points spanning 1386 sec, was divided into (in this case) four equal-length sections comprising 25 data points each. The four quartiles of the overall kinetic trace were fit to the straight line regression model. The corresponding quartile slopes (i.e., quartile

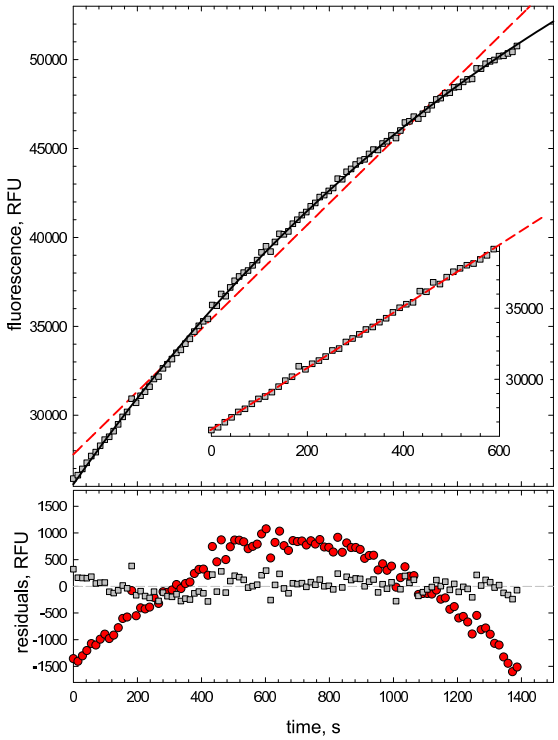

Figure 1: Time course of a typical EFGR L858R/T790M assay ($[E]_0$ = 20 nM, peptide $[S]_0$ = 13 μM, $[ATP]_0$ = 800 μM) in the absence of inhibitors. *Upper panel*: The grayed squares are the experimental data points; the solid curve represents the best least-squares fit to Eqn (13). The dashed line represents the results of linear least-squares regression. For details see text. *Upper panel - Inset*: Experimental data points spanning the first ten minutes of the assay. The dashed straight line was drawn by hand to emphasize apparent linearity. *Lower panel - Residual Plot*: The grayed squares represent residuals from the exponential fit of the experimental data to Eqn (13). The filled circles represent residuals from the linear fit.

reaction rates) are displayed as dashed line segments in *Fig* 2. Thus in the first quartile (t = 0 – 336 s) the reaction rate was 22.0 RFU/s; in the second quartile (t = 350 – 686 s) the reaction rate was 19.8 RFU/s; in the third quartile (t = 700 – 1036 s) the reaction rate was 15.6 RFU/s; and in the fourth quartile (t = 1050 – 1386 s) the reaction rate was 12.8 RFU/s. Thus the sectional reaction rate decreased by more than 40% from the first to the last quartile.

"Local" fit to the conventional algebraic model. The reaction progress curves from EGFR L858R/T790M assays conducted in the presence of varied amount of the inhibitor (Compound 5 from ref. [1]) were fit to Eqn (11). Each individual progress curve was analyzed separately ("local" as opposed to global [12] fit). The results for one of three independent replicates are summarized graphically in *Fig* 3. The overlay of experimental data (symbols) and the best-fit model (smooth curves) appears satisfactory on visual

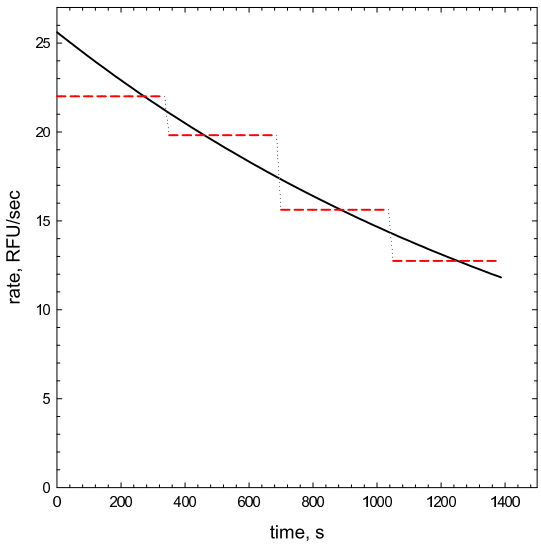

Figure 2: Changes of the observed reaction rate over time corresponding to the experimental data displayed in *Fig* 1. The smooth curve represents the first-derivatives, with respect to reaction time t, of the nonlinear reaction progress curve shown in *Fig* 1. The instantaneous rates were computed from Eqn (14) by using the best-fit parameter values, $F_{\max} = 45970$ RFU, and $k = 0.000557$ s^{-1}. The dashed line segments represent the slopes of straight lines fit to the four quartiles of the overall reaction progress curve. Thus the first dashed line segment represents the slope of a straight line fit to the first quartile ($t = 0$ through $t = 336$ s); the second straight line segment represents the the slope of a straight line fit to the second quartile ($t = 350$ s through $t = 686$ s); and so on.

inspection. The bottom panel shows the corresponding residual plots. The residuals exhibit only a relatively mild non-randomness, manifested as an inverted rainbow pattern spanning the first approximately 500 seconds of the assay. This is a consequence of a slight lag phase exhibited by many Omnia® kinase assays.

The best-fit values of optimized model parameters appearing in Eqn (11), v_{i} and k_{obs}, were averaged from three independently replicated determinations. The averaged ($n = 3$) values of k_{obs}, as well as the corresponding standard deviations from replicates, are summarized in Table 1.

Analysis of k_{obs} values derived from the conventional algebraic model. In an attempt to determine k_{inact}, K_{i} and $k_{\mathrm{inact}}/K_{\mathrm{i}}$ values using the conventional algebraic method [11], the k_{obs} values listed in Table 1 were fit to Eqn (12). The best-fit values of adjustable model parameters, and the associated formal standard errors from nonlinear regression, were $k_{\mathrm{inact}} = (0.91 \pm 0.10)$ ms^{-1} and $K_{\mathrm{i}} = (0.11 \pm 0.05)$ μM. Thus the corresponding best-fit value of the second-order rate constant $k_{\mathrm{inact}}/K_{\mathrm{i}}$ is (8.2 ± 3.4) mM^{-1}s^{-1}. In this case the formal standard error was computed by using error propagation theory [17]. See also Table 2, "Method A".

The coefficient of variation for $k_{\mathrm{inact}}/K_{\mathrm{i}}$ is approximately 40%, even though the pre-

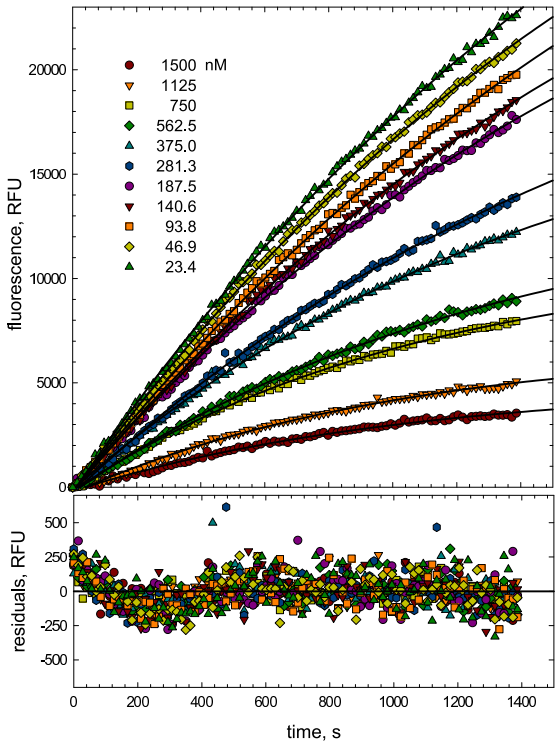

Figure 3: Representative time course of EGFR L858R/T790M ($[E]_0 = 20$ nM) inhibition by Compound 5 from ref. [1]. Symbols represent changes in experimentally observed fluorescence values at various inhibitor concentrations, as shown in the inset. Smooth curves represent the theoretical model generated by the least-squares fit to equation (11). Each individual curve was analyzed separately.

cision of the k_{obs} values used for the analysis is typically better than 10%. This is one particular indication of a lack of fit. The results are summarized graphically in *Fig* 4. The data points, representing experimentally determined k_{obs} values, clearly depart from the least-squares hyperbolic model curve, generated from Eqn (12). This is another indication of the fact that the hyperbolic model curve postulated by the conventional theory is not suitable in this case.

"Local" fit to the newly derived algebraic model. The reaction progress curves from EGFR L858R/T790M assays conducted in the presence of varied amount of the inhibitor (Compound 5 from ref. [1]) were fit to Eqn (1). Each individual progress curve was analyzed separately ("local" as opposed to global [12] fit). The overlay of the best-fit model curves superimposed on the experimental data points was virtually indistinguishable from the results obtained with Eqn (11), which are illustrated in *Fig* 3. The best-fit values of optimized model parameters appearing in Eqn (1), α and β, were averaged from three independently replicated determinations. The averaged ($n = 3$) values of the α parameter, as well as the corresponding standard deviations from replicates, are summarized in Table 1. A representative DynaFit script file is listed in

$[I]_0$, nM	k_{obs}, ms^{-1}	α, ms^{-1}
23.44	0.411 ± 0.050	0.048 ± 0.048
46.88	0.436 ± 0.044	0.088 ± 0.053
93.75	0.415 ± 0.036	0.112 ± 0.018
140.63	0.450 ± 0.044	0.168 ± 0.037
187.50	0.475 ± 0.049	0.213 ± 0.048
281.25	0.525 ± 0.088	0.327 ± 0.090
375.0	0.600 ± 0.058	0.430 ± 0.051
562.5	0.701 ± 0.035	0.578 ± 0.029
750.0	0.848 ± 0.088	0.746 ± 0.072
1125	0.927 ± 0.141	0.865 ± 0.139
1500	0.952 ± 0.145	0.907 ± 0.146

Table 1: Results of least-squares fit of individual progress curves to the conventional algebraic Eqn (12), column k_{obs}, or to the newly derived Eqn (1), column α. The best-fit values are averages from three separate determinations (i.e. three separate plate-reader plates). The plus-or-minus values are the corresponding standard deviations from independent replicates ($n = 3$).

Appendix A.

Analysis of α values derived from the newly derived algebraic model. In order to determine kinact, Ki and kinact/Ki values using the newly proposed algebraic method, the values listed in Table 1 were fitted to Eqn (2). The best-fit values of adjustable model parameters, and the associated formal standard errors from nonlinear regression, were $k_{inact} = (1.60 \pm 0.13)$ ms^{-1} and $K_i = (1.02 \pm 0.15)$ μM. Thus the corresponding best-fit value of the second-order rate constant k_{inact}/K_i is (1.6 ± 0.2) $mM^{-1}s^{-1}$. As before, the formal standard error of k_{inact}/K_i was computed by using error propagation theory [17]. The results are summarized graphically in *Fig* 5. See also Table 2, "Method B".

Global fit to the modified algebraic model. Eqn (1) was utilized to fit the progress curves displayed in *Fig* 3 in global regression mode [12]. In this approach all 11 progress curves were combined into a single super-set of experimental data. The globally optimized parameters were k_{kinact}, K_i, and k_{sub}. The locally optimized parameters, specific to each individual kinetic trace, were the baseline offset F_0 and the six highest inhibitor concentrations, $[I]_0$. A representative DynaFit script file is listed in Appendix B.

Partial optimization of the inhibitor concentrations was necessary because in preliminary analyses, when all inhibitor concentrations were treated as fixed constants, we observed serious deviations from randomness in the distribution of residuals. The reason is that the actual inhibitor concentrations are never exactly identical to the nominal inhibitor concentrations, due to unavoidable random errors in volume-delivery ("titration errors").

The three available replicates, each comprising 11 progress curves, were analyzed separately. The best-fit values of globally optimized parameters for the three independent replicates were k_{inact} = (0.00109, 0.00139, 0.00096) s^{-1} and K_i = (0.67, 0.86, 0.54) μM,

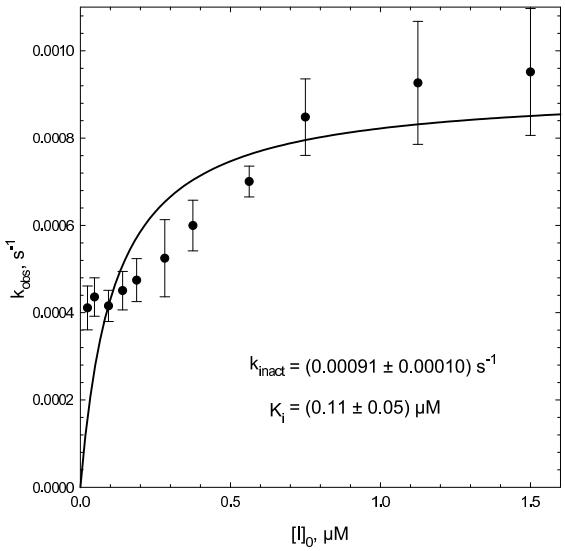

Figure 4: Least-squares fit of k_{obs} values obtained by using Eqn (11) to fit the reaction progress curves displayed in *Fig* 3. For further details see text.

respectively. Thus the three independently calculated values of the second-order inactivation rate constant were $k_{\mathrm{inact}}/K_{\mathrm{i}}$ = (0.0016, 0.0016, 0.0018) $\mu\mathrm{M}^{-1}\mathrm{s}^{-1}$. The averages and standard deviations from replicates (n = 3) are listed in the method-comparison Table 2 under "Method C".

Global fit to the general differential-equation model. The global super-set of combined reaction progress curves was fit to the differential equation model represented by Eqns (5)-(10), following the method used in a previous report [1]. The globally optimized parameters were the microscopic rate constants k_{sub}, k_{dI}, and k_{inact}. The locally optimized parameters, specific to each individual kinetic trace, were the baseline offset F_0 and the six highest inhibitor concentrations, $[I]_0$. The enzyme-inhibitor association rate constant k_{aI} was held fixed at 10 $\mu\mathrm{M}^{-1}\mathrm{s}^{-1}$. The best-fit value of the inhibition constant constant K_{i} was calculated as the ratio $k_{\mathrm{dI}}/k_{\mathrm{aI}}$. The three available replicates, each comprising 11 progress curves, were analyzed separately. The best-fit values of globally optimized parameters for the three independent replicates were k_{inact} = (0.00107, 0.00135, 0.00093) s^{-1} and K_{i} = (0.64, 0.82, 0.51) μM, respectively. Thus the three independently calculated values of the second-order inactivation rate constant were $k_{\mathrm{inact}}/K_{\mathrm{i}}$ = (0.00166, 0.00165, 0.00171) $\mu\mathrm{M}^{-1}\mathrm{s}^{-1}$. The averages and standard deviations from replicates (n = 3) are listed in the method-comparison Table 2 under "Method D".

4. DISCUSSION

Nonlinearity of the no-inhibitor control curve. The conventional fitting model for covalent enzyme inhibition, Eqn (11) (see ref. [11], Chapter 9), relies on the theoretical assumption that the control progress curve is linear over time. However, perfect

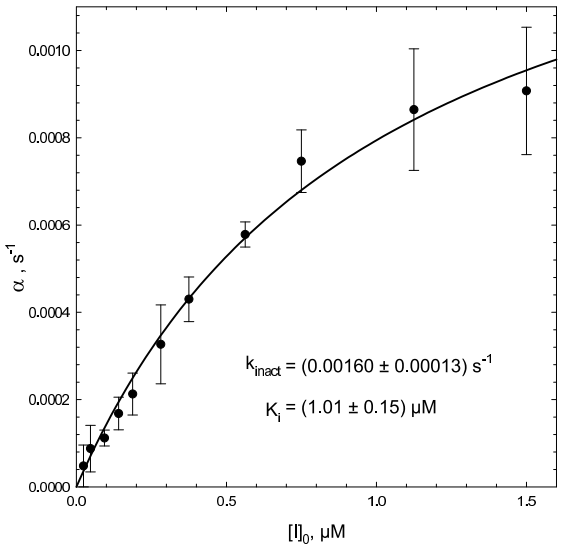

Figure 5: Least-squares fit of α values obtained by using Eqn (1) to fit the reaction progress curves displayed in *Fig* 3. For further details see text.

linearity is an unattainable ideal due to a variety of experimental factors such as enzyme deactivation or product inhibition. Such nuisance factors are more likely to be expressed in covalent inhibition assays, as compared to initial rate methods, because the assay times are necessarily prolonged to achieve substantial irreversible inactivation. Therefore the two relevant questions are, first, what particular degree of nonlinearity in the control curve is acceptable and, second, how best to measure it. In any given case the answers will determine whether it is justified to use the conventional fitting model for covalent inhibition, Eqn (11), or whether it is necessary to employ either the newly derived algebraic Eqn (1) or even the full ODE model represented by Eqns (5)-(10).

Discussions with practitioners in both academia and industry regarding the results presented in this paper revealed a widely divergent spectrum of opinions on the linearity

Method	k_{inact}, ms^{-1}	K_{i}, μM	$k_{\mathrm{inact}}/K_{\mathrm{i}}$, mM^{-1} s^{-1}
A	0.91 ± 0.11	0.11 ± 0.05	8.2 ± 3.9
B	1.60 ± 0.13	1.02 ± 0.15	1.57 ± 0.26
C	1.07 ± 0.22	0.66 ± 0.16	1.62 ± 0.08
D	1.09 ± 0.21	0.65 ± 0.15	1.69 ± 0.09

Table 2: Final results - comparison of methods. The plus-or-minus values for methods "A" and "B" (local fit) are formal standard errors from nonlinear regression of averaged kobs or values, respectively. The plus-or-minus values for methods "C" and "D" (global fit) are standard deviations from independent replicates (n = 3). For further details see text.

vs. nonlinearity of raw data such as those displayed in *Fig* 1. Some investigators focused on the inset plot and concluded that the entire 24-minute curve is probably "linear enough" to justify the use of the conventional fitting model, because the first ten minutes of the assay appear "perfectly linear" by visual inspection. Other researchers focused on the residual plots but were skeptical of the instantaneous rate plots in *Fig* 2. The claim of "sufficient linearity" of the control curve in *Fig* 1 is seemingly bolstered by the fact that R-squared value from linear regression is relatively high ($R^2 = 0.99$). Indeed some investigators mistakenly believe that the R^2 value measures the "goodness of fit between theoretical curves and experimental data" [18]. In fact, R^2 measures how *strongly* the dependent variable, in this case fluorescence intensity, varies with the independent variable, in this case reaction time. However the qualitative *nature* of this dependence – e.g. "goodness of fit" to a linear, exponential, hyperbolic, or another fitting model – is not reflected in R^2 at all. That is why it is possible to observe $R^2 = 0.99$ (presumably a "good fit") and a decidedly nonrandom distribution of residuals (a "poor fit", as seen in the bottom panel of *Fig* 1).

To complicate the matters further, our own experience shows that the randomness in the distribution of residuals, when considered in isolation, is not a suitable measure of significant nonlinearity in enzyme kinetics. If fact, we found that in certain exquisitely well-tuned enzyme assays [19] the random scatter in the data points is so low that even insignificant departures from linearity (e.g. those observed at extremely low final substrate conversions) will produce decidedly nonrandom residual patterns.

Based on similar practical reasons, we hereby propose an operational definition of nonlinearity in the context of covalent enzyme inhibition kinetics, which is inspired by the "cross-validation" concept from statistics [16]. The basic idea is to divide the control progress curve into two halves; fit each segment to the straight line model; and finally compare the two resulting slopes, i.e., the "initial" and "final" reaction rates. If the reaction rates in the first half and in the second half differ by more than 20%, the entire progress curve should be declared operationally nonlinear. Other cut-off values (25% or 33%) are possible and will depend on the particular project. *Fig* 2 illustrates a small variation on this theme, where we used four instead of two equal-length segments.

Comparison of methods. In this work we compared four data-analytic methods for the determination of k_{inact}, K_{i}, and $k_{\mathrm{inact}}/K_{\mathrm{i}}$. Method "A" represents the conventional approach based on the algebraic equation (11) [11]. This method is based on two underlying assumptions. The first assumption, unambiguously satisfied in the case of Compound 5 [1], is that there is no "tight binding" [4] in the sense that the inhibition constant of the initial noncovalent complex is very much larger than the active enzyme concentration. The second assumption underlying method "A" is that the no-inhibitor control progress curve is linear over time, corresponding to constant reaction rate over the entire course of the assay. However, perfect linearity is not achievable, which is why the main goal of this report was to determine whether or not the particular degree of nonlinearity displayed in *Fig* 1 might have a significant effect on k_{inact}, K_{i}, and $k_{\mathrm{inact}}/K_{\mathrm{i}}$.

Three alternate methods of analysis, namely methods "B" through "D" listed in Table 2, were chosen for unbiased comparison with the conventional method "A". Methods "B" and "C", identically to method "A", also assume that that the there is no tight binding but, in opposition to method "A", assume that the substrate concentration is very much lower than the corresponding Michaelis constant and therefore that the no-inhibitor control is exponential rather than linear. In our case the peptide substrate concentra-

tion was $[S]_0 = 13\ \mu$M while $K_{\mathrm{M,Pep}} > 200\ \mu$M [1], therefore exponential time course of the no-inhibitor control is to be expected from theory. Finally, method "D" makes no assumptions about the strength of initial binding, in the sense that it treats indiscriminately both inhibitors that are "tight binding" in the initial complex and inhibitors that are only weakly bound.

A comparison of methods "C" (global algebraic) and "D" (global differential) shows that the results for all three kinetic constants (k_{inact}, K_{i}, and $k_{\mathrm{inact}}/K_{\mathrm{i}}$) are virtually identical. This provides an important validation of the newly derived algebraic Eqn (1) because – to repeat for emphasis – method "D" makes no assumption about the presence or absence of tight binding and in that sense it is the most unbiased of the four methods being compared.

A comparison of methods "B" (local algebraic) and "C" (global algebraic), both of which are based on Eqn (1), shows that the these two methods provide virtually identical results for $k_{\mathrm{inact}}/K_{\mathrm{i}}$, whereas the local fit method "B" appears to overestimate both (k_{inact} and K_{i} by approximately 40%. It should be noted that global analysis of biochemical and biophysical data was repeatedly shown to be superior to the stepwise, local fit method [12], which is why we place greater confidence in method "C" as compared with method "B".

Comparison of methods "A" and "B", which are otherwise identical except for the use of the algebraic Eqns (11) or (1), respectively, shows that the conventional method "A" performed reasonably well in terms of the first-order inactivation rate constant k_{inact}. The average from three independent replicates was $k_{\mathrm{inact}} = 0.0009\ \mathrm{s}^{-1}$, whereas methods "B" through "D" yielded $k_{\mathrm{inact}} = 0.0016$, 0.0012, and $0.0011\ \mathrm{s}^{-1}$, respectively. Thus the inactivation rate constant is underestimated by method "A" by at most 50%. However, the best-fit value of K_{i} was severely distorted by ignoring the presumably "slight" nonlinearity present in the no-inhibitor control. In particular, the conventional method "A" produced $K_{\mathrm{i}} = 0.1\ \mu$M whereas methods "B" using the more appropriate algebraic model resulted in $K_{\mathrm{i}} = 1.0\ \mu$M. This represents an order-of-magnitude distortion. The unbiased global fit method "D" resulted in $K_{\mathrm{i}} = 0.7\ \mu$M, a sevenfold difference as compared to the conventional method "A". Similar distortion or bias in the results from method "A" was seen for the second-order deactivation rate constant $k_{\mathrm{inact}}/K_{\mathrm{i}}$.

In conclusion, the "almost perfect" linearity of the no-inhibitor control curve displayed in *Fig* 1 can rightly be characterized as an optical illusion. To the untrained eye it would appear that the reaction rate is constant at least over the first ten minutes of the assay. However, the actual nonlinearity is clearly revealed in *Fig* 2, which shows that the slope (i.e., reaction rate) changes significantly between the first five minutes and the second five minutes of the assay. More importantly this rather subtle nonlinearity (almost undetectable by naked eye) has a decidedly non-subtle effect on the final value of K_{i} amounting to an order-of-magnitude distortion, as shown in Table 2.

The role of ATP as co-substrate. The newly derived algebraic Eqn (1) does not explicitly take into account that protein kinase assays include ATP as a co-substrate. However, ATP presence is implied in the semantics of the dissociation constant K_{i}. In particular, K_{i} in Eqns (2) and (3) should be viewed as an "apparent K_{i}", as defined by Cha [4] and others. For example, if the given kinase inhibitor is kinetically competitive with respect to ATP, then the "true Ki" of the inhibitor can be computed from the "apparent K_{i}" determined from Eqn (1) as $K_{\mathrm{i}}/(1 + [ATP]/K_{\mathrm{M,ATP}})$. This is the treatment we utilized for Compound 5 (an ATP-competitive inhibitor) in a previously published

report [1]. However, in this paper we report only the "apparent" K_i values.

Limitations of the newly presented algebraic model. The algebraic fitting model represented by the newly derived integrated rate Eqn (1) is applicable only if two simplifying assumptions are satisfied at the same time. First, the peptide substrate concentration must be very much lower than the corresponding Michaelis constant. Second, the inhibition constant that describes the initially formed noncovalent enzyme-inhibitor complex must be very much larger than the active enzyme concentration.

The low substrate requirement ($[S]_0 << K_\mathrm{M}$) does not seem overly restrictive, because in many practically important cases the substrate concentration in fact necessarily remains very low relative to the corresponding K_M, due to low solubility, inner filtration effects [20], or other experimental constraints.

The low potency and/or low enzyme concentration requirement ($[E]_0 < K_\mathrm{i}$) does not appear overly onerous either. Especially in the relatively early stages of preclinical discovery, the biochemical analyst is likely to be faced with many low-affinity enzyme inhibitors. In favorable cases, the experimental setup can be adjusted such that the active enzyme concentration can be lowered to single-digit picomolar concentrations without a catastrophic loss of overall sensitivity. Under those circumstances the algebraic rate equations presented here could be used to characterize even highly potent ($K_\mathrm{i} > 10$ pM) covalent enzyme inhibitors.

Lastly, it should be noted that an effective application of the newly derived kinetic model represented by Eqn (1) requires prior independent determination of the molar response factor of the reaction product, r_P, which must subsequently be kept constant in the regression analysis. As a reminder, the response factor is defined simply as the number of arbitrary instrument units (for example, absorbance units or relative fluorescence units) corresponding to the given concentration unit (for example, one micromole per liter) of the final reaction product being formed in the enzyme reaction. Fortunately this particular quantity can be easily determined in a variety of ways.

In conclusion, differential-equation modeling of experimental kinetic data does remain the most universally applicable mathematical formalism, because it makes no simplifying assumptions. Nevertheless, regardless of its relatively narrow utility, the algebraic model for covalent inhibition kinetics presented in this report should add a useful tool into the biochemical analyst's toolbox.

ACKNOWLEDGMENTS

We thank Bob Copeland (Epizyme, Inc., Cambridge, Massachusetts) and Art Wittwer (Confluence Life Sciences, Inc., St. Louis, Missouri) for helpful discussions during the preparation of this manuscript.

References

[1] P. A. Schwartz, P. Kuzmic, J. Solowiej, S. Bergqvist, B. Bolanos, C. Almaden, A. Nagata, K. Ryan, J. Feng, D. Dalvie, J. Kath, M. Xu, R. Wani, B. W. Murray, Covalent EGFR inhibitor analysis reveals importance of reversible interactions to potency and mechanisms of drug resistance, Proc. Natl. Acad. Sci. U.S.A. 111 (2014) 173–178.

[2] P. Kuzmic, Program DYNAFIT for the analysis of enzyme kinetic data: Application to HIV proteinase, Anal. Biochem. 237 (1996) 260–273.

[3] P. Kuzmic, DynaFit - A software package for enzymology, Meth. Enzymol. 467 (2009) 247–280.

[4] S. Cha, Tight-binding inhibitors. I. Kinetic behavior, Biochem. Pharmacol. 24 (1975) 2177–2185.
[5] S. Cha, R. P. Agarwal, R. E. Parks, Tight-binding inhibitors. II. Non-steady state nature of inhibition of milk xanthine oxidase by allopurinol and alloxanthine and of human erythrocyte adenosine deaminase by coformycin, Biochem. Pharmacol. 24 (1975) 2187–2197.
[6] S. Cha, Tight-binding inhibitors. III. A new approach for the determination of competition between tight-binding inhibitors and substrates–inhibition of adenosine deaminase by coformycin., Biochem. Pharmacol. 25 (24) (1976) 2695–702.
[7] S. Cha, Tight-binding inhibitors. VII. Extended interpretation of the rate equation, experimental designs and statistical methods, Biochem. Pharmacol. 29 (1980) 1779–89.
[8] S. Cha, S. Y. R. Kim, S. G. Kornstein, P. W. Kantoff, K. H. Kim, F. N. M. Naguib, Tight-binding inhibitors. IX. Kinetic parameters of dihydrofolate reductase inhibited by methotrexate, an example of equilibrium study, Biochem. Pharmacol. 30 (1981) 1507–15.
[9] J. F. Morrison, Kinetics of the reversible inhibition of enzyme-catalysed reactions by tight-binding inhibitors, Biochim. Biophys. Acta 185 (1969) 269–286.
[10] S. Szedlacsek, R. G. Duggleby, Kinetics of slow and tight-binding inhibitors, Meth. Enzymol. 249 (1995) 144–180.
[11] R. A. Copeland, Evaluation of Enzyme Inhibitors in Drug Discovery, Second Edition, John Wiley, New York, 2013.
[12] J. M. Beechem, Global analysis of biochemical and biophysical data, Meth. Enzymol. 210 (1992) 37–54.
[13] A. C. Hindmarsh, ODEPACK: a systematized collection of ODE solvers, in: R. S. Stepleman, M. Carver, R. Peskin, W. F. Ames, R. Vichnevetsky (Eds.), Scientific Computing, North Holland, Amsterdam, 1983, pp. 55–64.
[14] B. Mannervik, Regression analysis, experimental error, and statistical criteria in the design and analysis of experiments for discrimination between rival kinetic models, Meth. Enzymol. 87 (1982) 370–390.
[15] J.-G. Reich, Curve Fitting and Modeling for Scientists and Engineers, McGraw-Hill, New York, 1992.
[16] G. Wahba, S. Wold, A completely automatic french curve: fitting spline functions by cross validation, Comm. Statistics 4 (1975) 1–17.
[17] P. R. Bevington, Data Reduction and Error Analysis in the Physical Sciences, McGraw-Hill, New York, 1969.
[18] A. Chang, J. Schiebe, W. Yu, G. R. Bommineni, P. Pan, M. V. Baxter, A. Khanna, C. A. Sotriffer, C. Kisker, P. J. Tonge, Rational optimization of drug-target residence time: Insights from inhibitor binding to the staphylococcus aureus fabi enzyme-product complex, Biochemistry 52 (2013) 4217–4228.
[19] J. A. Kenniston, R. R. Faucette, D. Martik, S. R. Comeau, A. P. Lindberg, K. J. Kopacz, G. P. Conley, J. Chen, M. Viswanathan, N. Kastrapeli, J. Cosic, S. Mason, M. DiLeo, J. Abendroth, P. Kuzmic, R. C. Ladner, T. E. Edwards, C. TenHoor, B. A. Adelman, A. E. N. and, D. J. Sexton, Inhibition of plasma kallikrein by a highly specific active site blocking antibody, J. Biol. Chem. 289 (2014) 23596–23608.
[20] Y. Liu, W. Kati, C. Chen, R. Tripathi, A. Molla, W. Kohlbrenner, Use of a fluorescence plate reader for measuring kinetic parameters with inner filter effect correction, Anal. Biochem. 267 (1999) 331–5.

APPENDIX

This Appendix lists DynaFit scripts implementing the algebraic fit to Eqn (1). The coding below can be easily adapted for any software package that allows the user to specify an arbitrary algebraic fitting model, such as SigmaPlot, ORIGIN, GraphPad Prism, and others. The raw data file sheet.txt, referred to in the DynaFit scripts listed below, is available for download from http://www.biokin.com/.

A. "Local" fit of reaction progress curves to Eqn (1)

The following DynaFit script represents "local" fit of Compound 5 inhibition data to the algebraic model represented by Eqn (1). In this case only the first of three replicates

("R1" in the coding below) was analyzed. However the kinetic analysis was performed identically for all three independent replicates. The symbols "a" and "b" below stand for the model parameters α and β, respectively.

```
[task]
   task = fit
   data = generic
[parameters]
   t, Fo, a, b
[model]
   So = 13
   rP = 4500
   a = 0.001 ?
   b = 0.1 ?
   P = So*(1 - exp(-b*(1-exp(-a*t) ) ) )
   Fo = -100 ? (-2000 .. +2000)
   F = Fo + rP * P
[data]
   variable  t
   directory ./Cpd-5/R1/data
   sheet     sheet.txt
column 2
[output]
   directory ./Cpd-5/R1/output/algloc-001
[settings]
{Filter}
  ZeroBaselineSignal = y
[task] | data = generic | task = fit | [data] | variable t | column 3
[task] | data = generic | task = fit | [data] | variable t | column 4
[task] | data = generic | task = fit | [data] | variable t | column 5
[task] | data = generic | task = fit | [data] | variable t | column 6
[task] | data = generic | task = fit | [data] | variable t | column 7
[task] | data = generic | task = fit | [data] | variable t | column 8
[task] | data = generic | task = fit | [data] | variable t | column 9
[task] | data = generic | task = fit | [data] | variable t | column 10
[task] | data = generic | task = fit | [data] | variable t | column 11
[task] | data = generic | task = fit | [data] | variable t | column 12
[end]
```

B. Global fit of reaction progress curves to Eqn (1)

The following DynaFit script represents global ft of Compound 5 inhibition data to the algebraic model represented by Eqn (1). This script applies to the first of three replicates ("R1" in the coding below).

```
[task]
   task = fit
   data = generic
[parameters]
   t, Eo, So, Io, ksub, Ki, kinact, Fo, rP
```

```
[model]
   Eo = 0.02
   So = 13
   Ki = 1 ?
   kinact = 0.01 ?
   ksub = 0.001 ?
   rP = 4500
   a = kinact * Io/(Io + Ki)
   b = (Eo*ksub/kinact) * (Ki/Io)
   P = So*(1 - exp(-b*(1-exp(-a*t) ) ) )
   F = Fo + rP * P
[data]
   variable  t
   directory ./Cpd-5/R1/data
   sheet     sheet.txt
column  2 | param Fo = -500 ? (-2000 .. +2000), Io = 1.5 ?
column  3 | param Fo = -500 ? (-2000 .. +2000), Io = 1.125 ?
column  4 | param Fo = -500 ? (-2000 .. +2000), Io = 0.75 ?
column  5 | param Fo = -500 ? (-2000 .. +2000), Io = 0.5625 ?
column  6 | param Fo = -500 ? (-2000 .. +2000), Io = 0.375 ?
column  7 | param Fo = -500 ? (-2000 .. +2000), Io = 0.28125 ?
column  8 | param Fo = -500 ? (-2000 .. +2000), Io = 0.1875
column  9 | param Fo = -500 ? (-2000 .. +2000), Io = 0.140625
column 10 | param Fo = -500 ? (-2000 .. +2000), Io = 0.09375
column 11 | param Fo = -500 ? (-2000 .. +2000), Io = 0.046875
column 12 | param Fo = -500 ? (-2000 .. +2000), Io = 0.0234375
[output]
   directory ./Cpd-5/R1/output/algeb-001
[settings]
{Filter}
   ZeroBaselineSignal = y
[end]
```

C. Derivation of Eqn (1)

Let us assume that a covalent inhibition assay is conducted under the special experimental conditions where the substrate concentration $[S]_0$ is very much lower than Michaelis constant K_M. It has been shown that under those conditions the kinetic mechanism can be represented by the "hit-and-run" model shown in Scheme 1. Please note that the Michaelis complex E.S is not represented in Scheme 1, because its mole fraction is assumed to be negligibly small.

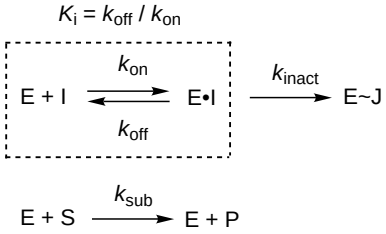

Scheme 1

According to Scheme 1, the formation of the covalent conjugate E∼I over time is governed by the differential equation (C.1), where $[E.I]$ is the concentration of the non-covalent complex at the reaction time t.

$$\frac{\mathrm{d}[E{\sim}I]}{\mathrm{d}t} = k_{\mathrm{inact}}[E.I] \tag{C.1}$$

Invoking the rapid-equilibrium approximation we can define the equilibrium dissociation constant of the initial noncovalent complex as $K_{\mathrm{i}} = [I][E]/[E.I]$. However, assuming that K_{i} is very much larger than the active enzyme concentration (no "tight binding" and no inhibitor depletion) allows us to substitute the total or analytic inhibitor concentration, $[I]_0$, for the free equilibrium concentration, $[I]$. Thus $[E.I] = [I]_0\,[E]/K_{\mathrm{i}}$ and therefore Eqn (C.1) can also be written as shown in Eqn (C.2).

$$\frac{\mathrm{d}[E{\sim}I]}{\mathrm{d}t} = k_{\mathrm{inact}}[E]\frac{[I]_0}{K_{\mathrm{i}}} \tag{C.2}$$

The mass balance for enzyme forms can be written as shown in Eqn (C.3). Note that the Michaelis complex concentration $[E.S]$ is neglected in the mass balance equation, due to the special conditions whereby $[S]_0 << K_{\mathrm{M}}$. The concentration of the covalent conjugate can thus be expressed as shown in Eqn (C.4).

$$[E]_0 = [E] + [E.I] + [E{\sim}I] = [E]\left(1 + \frac{[I]_0}{K_{\mathrm{i}}}\right) + [E{\sim}I] \tag{C.3}$$

$$[E{\sim}I] = [E]_0 - [E]\left(1 + \frac{[I]_0}{K_{\mathrm{i}}}\right) \tag{C.4}$$

Differentiating both sides of Eqn ((C.4)) with respect to the reaction time, t, we obtain Eqn (C.5).

$$\frac{\mathrm{d}[E{\sim}I]}{\mathrm{d}t} = -\frac{\mathrm{d}[E]}{\mathrm{d}t}\left(1 + \frac{[I]_0}{K_{\mathrm{i}}}\right) \tag{C.5}$$

The right-hand sides of Eqns (C.1) and (C.5) must be equal, which leads, after a trivial rearrangement, to the differential equation (C.6) for the rate of change in the free enzyme concentration $[E]$ as it evolves over time.

$$\frac{\mathrm{d}[E]}{\mathrm{d}t} = -k_{\mathrm{inact}}[E]\frac{[I]_0}{[I]_0 + K_{\mathrm{i}}} \tag{C.6}$$

Equation (C.6) can be integrated in a closed form after the separation of variables as shown in Eqn (C.7), where $[E](0)$ is the free enzyme concentration at time zero.

$$\int_{[E](0)}^{[E]} \frac{\mathrm{d}[E]}{[E]} = -k_{\mathrm{inact}}\frac{[I]_0}{[I]_0 + K_{\mathrm{i}}}\int_0^t \mathrm{d}t \tag{C.7}$$

The definite integral on the right-hand side of Eqn (C.7) can evaluated simply as $\int_0^t \mathrm{d}t = t$. Let us introduce an auxiliary constant α defined as shown in Eqn (C.8). Then the integral equation (C.7) can be rewritten as shown in Eqn (C.9).

$$\alpha \equiv k_{\mathrm{inact}} \frac{[I]_0}{[I]_0 + K_{\mathrm{i}}} \tag{C.8}$$

$$\int_{[E](0)}^{[E]} \frac{\mathrm{d}[E]}{[E]} = -\alpha\, t \tag{C.9}$$

Importantly, based on the rapid equilibrium approximation, the lower integration bound for the free enzyme concentration, $[E](0)$ in Eqn (C.9), which is the free enzyme concentration at time zero (as opposed to total or analytic concentration $[E]_0$), can be expressed as shown in Eqn (C.10).

$$[E](0) = [E]_0 \frac{K_{\mathrm{i}}}{[I]_0 + K_{\mathrm{i}}} \tag{C.10}$$

Thus the definite integral in Eqn (C.9) can be evaluated as shown in Eqn (C.11) and the free enzyme concentration, [E], evolves over time according to Eqn (C.12).

$$\ln[E] - \ln\left([E]_0 \frac{K_{\mathrm{i}}}{[I]_0 + K_{\mathrm{i}}}\right) = -\alpha\, t \tag{C.11}$$

$$[E] = [E]_0 \frac{K_{\mathrm{i}}}{[I]_0 + K_{\mathrm{i}}} \exp\left(-\alpha\, t\right) \tag{C.12}$$

According to the "hit-and-run" mechanism postulated in Scheme 1 (see also ref. [1]) the rate of change in the substrate concentration is expressed by the differential Eqn (C.13).

$$\frac{\mathrm{d}[S]}{\mathrm{d}t} = -k_{\mathrm{sub}}[E][S] \tag{C.13}$$

After the separation of variables and after substitution for [E] from Eqn (C.12), we obtain the integral equation (C.14).

$$\int_{[S]_0}^{[S]} \frac{\mathrm{d}[S]}{[S]} = -k_{\mathrm{sub}}[E]_0 \, \frac{K_{\mathrm{i}}}{[I]_0 + K_{\mathrm{i}}} \int_0^t \exp\left(-\alpha\, t\right) \tag{C.14}$$

Analytic integration of both sides of Eqn (C.14), within the indicated bounds, leads directly to Eqn (C.15) expressing changes in the substrate concentration, $[S]$, over the reaction time, t.

$$[S] = [S]_0 \, \exp\left\{-\frac{k_{\mathrm{sub}}[E]_0}{[I]_0 + K_{\mathrm{i}}} \, \frac{K_{\mathrm{i}}}{\alpha} \left[1 - \exp\left(-\alpha\, t\right)\right]\right\} \tag{C.15}$$

For convenience we can introduce the auxiliary variable β defined as shown in Eqn (C.16). The reaction product concentration can be computed as $[P] = [S]_0 - [S]$, which leads to Eqn (C.17). Finally, introducing the baseline experimental signal F_0 and the assuming that the observed signal intensity is proportional to the product concentration $[P]$ via the molar response coefficient, r_{P}, we obtain Eqn (C.18) which is equivalent to Eqn (1) above.

$$\beta \equiv \frac{k_{\mathrm{sub}}[E]_0}{[I]_0 + K_{\mathrm{i}}} \; \frac{K_{\mathrm{i}}}{\alpha} = \frac{k_{\mathrm{sub}}[E]_0}{k_{\mathrm{inact}}} \; \frac{K_{\mathrm{i}}}{[I]_0} \tag{C.16}$$

$$[P] = [S]_0 \; \exp\left\{1 - \beta\left[1 - \exp\left(-\alpha\, t\right)\right]\right\} \tag{C.17}$$

$$F = F_0 + r_{\mathrm{P}}\,[P] \tag{C.18}$$